Mixing properties of Al 2 O 3 (0001)-supported M 2 O 3 and MM'O 3 monolayers (M, M' = Ti, V, Cr, Fe)

C. Noguera, J. Goniakowski

Mixing properties of $Al_2O_3(0001)$-supported M_2O_3 and $MM'O_3$ monolayers (M, M′=Ti, V, Cr, Fe)

C. Noguera, J. Goniakowski

‡

CNRS-Sorbonne Université, UMR 7588, INSP, F-75005 Paris, France

Abstract. Considering the importance of sub-monolayer transition metal oxides supported on another oxide in many industrial processes, with the help of a DFT+U approach, we provide information on the structural and electronic properties of pure M_2O_3 and mixed MM'O_3 $3d$ monolayers (M, M' = Ti, V, Cr, Fe) supported on an α-$Al_2O_3(0001)$ support. With their structure in the prolongation of the alumina corundum lattice, the monolayers have non-equivalent surface and interface cations which leads to two different cation configurations in the mixed oxides. In all cases, the interfacial charge transfer is weak, but strong cation-cation electron redistributions may take place as in $TiVO_3$, $TiFeO_3$, $VFeO_3$, and $TiCrO_3$ in which actual redox processes lead to oxidation states different from the expected +3 value. We show that the tendency to mixing relies on the interplay between two very different driving forces. Cation-cation redox reactions, in most cases, strongly stabilise mixed configurations, but preference for a given cation position in the monolayer because of surface energy reasons may strengthen, weaken or even block the mixing tendency. By comparison with results obtained in bulk ilmenite, in free-standing monolayers and in MLs deposited on transition metal substrates, we evidence the flexibility of their electronic structure as a function of size, dimensionality and nature of support, as a lever to tune their properties for specific applications.

‡ e.mail: jacek.goniakowski@insp.jussieu.fr, claudine.noguera@insp.jussieu.fr

1. Introduction

Reducible transition metal (TM) sesquioxides M_2O_3 of corundum structure are involved in numerous natural or industrial processes. For example, hematite Fe_2O_3 is omnipresent in the natural environment where it helps fixing contaminants, and also finds applications in electrochemical water splitting. Eskolaite Cr_2O_3 is an efficient catalyst and an important constituent of many ceramics. It acts as a protective layer against corrosion on iron surfaces. Apart from its role as a catalyst, V_2O_3 displays a metal-insulator (MI) transition as a function of temperature which is used in energy related applications.

These properties may be tuned by doping the oxides or varying their thickness in thin film geometry. M_2O_3 thin films have been synthesized on various substrates, whether metallic or insulating [1]. In the latter case, the choice of c-cut sapphire α-Al_2O_3(0001) is especially beneficial, due to its stability, its high surface quality, and the similarity of its structure to that of the TM sesquioxides. There are numerous examples of M_2O_3 thin film growth on it, for example Ti_2O_3 [2], V_2O_3 [3, 4], Cr_2O_3 [5], Fe_2O_3 [6] or sesquioxides resulting from the oxidation of stainless steel buffers intended to favour adhesion of anti-corrosive galvanic zinc coatings [7, 8]. The same is true for some mixed oxides such as $(Fe_{1-x}V_x)_2O_3$ [9], $(Cr_{1-x}Al_x)_2O_3$ [10], or $VTiO_3$ [11].

The incorporation of dopants in corundum oxides is also a lever to obtain new functionalities. Multicomponent oxides display flexible structural and electronic characteristics as a function of the relative concentration of their components, the particle size, the film thickness and the nature of the support on which they are synthesized [1]. Compared to their pure analogues, mixed oxides sometimes simply combine the advantages of the parent oxides, but in some cases, they may also exhibit unexpected new features. It was, for example, shown that Cr-doping changes the V_2O_3 MI transition temperature [12], that Mn-doping modifies the H_2 adsorption on α-Al_2O_3 [13], or that optical properties of α-Al_2O_3 are sensitive to TM atom doping [14]. Recently, we have shown that the contact between two M_2O_3 oxides [15] or their mixing, whether in the bulk [16] or at the monolayer (ML) limit [17, 18, 19] may induce a change of cation oxidation states, with strong implications on their electronic and reactivity properties.

M_2O_3 thin films at the ultimate ML limit have been extensively studied experimentally and theoretically, whether supported on Pd(111) [20, 21], on Pt(111) [22, 23], or on Au(111) [24, 21, 18, 25, 26, 27, 28]. However, apart from MLs inserted into α-Al_2O_3 [29, 30], fewer works have envisioned the properties of TM sesquioxide MLs on the α-Al_2O_3(0001) surface.

This is the subject of the present theoretical work, which considers both pure M_2O_3 and mixed MM'O_3 MLs with M, M'=Ti, V, Cr and Fe. We show that their structure, in continuation of the corundum lattice, is far from the quasi-planar geometry found on metal substrates, that the interfacial charge transfer is weak, and that segregation effects are present in the mixed MLs with preferential presence of one or the other cation at the surface. Strong electron redistributions, which can be considered as actual redox processes leading to changes of cation oxidation states, take place between the TM cations in several mixed compounds, such as in $TiVO_3$, $TiFeO_3$, $VFeO_3$, and $TiCrO_3$. We show that the mixing tendency, i.e. the stability of the mixed MLs with respect to their parent oxides, depends on the interplay between two physical processes, namely change of oxidation state and surface under-coordination. When comparing the present results to those obtained previously for the same mixed oxides in different morphologies or environments, we conclude that these electronic characteristics are strongly dependent on size, dimensionality and nature of support, which suggests routes to tune TM oxide ML properties for specific applications

The paper is organized as follows. After a section devoted to the computational method and set-up (Sec. 2), we report results on Al_3O_3-supported pure M_2O_3 MLs (Sec. 3) and mixed MM'O_3 MLs (Sec. 4). These results are then discussed in Sec. 5, before a conclusion.

2. Computational details

DFT calculations have been performed with the Vienna Ab-initio Simulation Package (VASP) [31, 32] using the Projector Augmented Wave (PAW) method [33, 34] to represent the electron-core interaction and a 400 eV energy cut-off in the development of Kohn-Sham orbitals on a plane-wave basis set. As in our previous studies, [16, 15, 17, 18] a dispersion-corrected (optB88-vdW) [35, 36, 37] exchange-correlation functional has been employed, within the DFT+U ap-

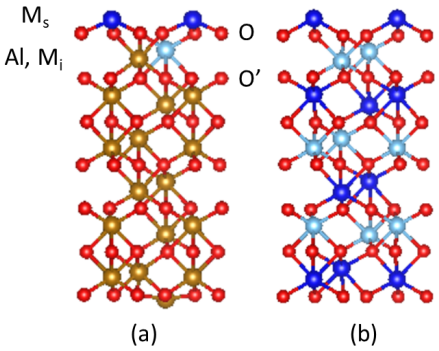

Figure 1. Profile views of the atomic structures of (a) an Al_2O_3-supported MM'O_3 ML, and (b) a bulk MM'O_3 oxide in the ilmenite structure. M and M' cations, oxygen atoms and Al cations are represented by light and dark blue, red, and golden balls, respectively. Subscripts i and s refer to the ML interface and surface cations, respectively.

proach proposed by Dudarev [38, 39] with U values close to those reported in the literature: $U = 1$ eV for Ti_2O_3, $U = 1.7$ eV for V_2O_3, $U = 3$ eV for Cr_2O_3 and Fe_2O_3. Moreover we have performed complementary calculations using the HSE03 hybrid approach with 1/4 of the short-range Hartree-Fock exact exchange, and range-separation parameter equal 0.3 Å^{-1}, [40, 41] to test the sensitivity of our results to the choice of the exchange-correlation functional (Supporting Information (SI), Sections S2-S4).

All calculations are spin-polarized and the relative stability of simple non-magnetic (NM) and magnetic solutions (with either parallel (FM) or anti-parallel (AF) TM spin moments) has been systematically tested. Ionic charges are estimated with the partition scheme proposed by Bader [42, 43] and magnetic moments are obtained by integration of the spin density within the Bader's volumes. The oxide ML and alumina substrate charges are evaluated as a sum of all the respective ionic charges and the interface charge transfer is deduced from the non-neutrality of the alumina substrate. Atomic configurations are plotted with VESTA [44].

We have considered pure M_2O_3 (the parents) and mixed MM′O_3 monolayers (M, M′ = Ti, V, Cr, and Fe), supported on α-Al_2O_3(0001), in the prolongation of the corundum structure, Figure 1a. The Al_2O_3 substrate is represented by a six Al-O_3-Al trilayer thick slab terminated by a single Al atom on each side (non-polar terminations), and the oxide films are deposited on one side of the support. They are modelled with a single M_2O_3 or MM′O_3 formula unit (f.u.) in an Al_2O_3(0001) (1×1) unit cell at the Al_2O_3 bulk lattice parameter (4.75 Å). The sampling of the Brillouin zone is performed with the Γ-centred $(8 \times 8 \times 1)$ Monkhorst-Pack mesh [45].

All atomic coordinates are allowed to fully relax until forces get lower than 0.01 eVÅ^{-1}. In the following, the atomic or electronic characteristics of these supported MLs will be compared to those of corundum M_2O_3 or ilmenite MM'O_3 bulk structures [16] (Figure 1b). DFT+U results for the M_2O_3 bulks and free (0001) surfaces are recalled in SI, Section S1.

Table 1. Main structural and electronic characteristics of Al_2O_3-supported M_2O_3 MLs: interplane distances d within the ML (Å), cation charge Q_M (e), oxygen charge in the ML Q_O (e), total substrate charge $Q_{Al_2O_3}$ (e/surface unit cell), cation magnetic moment μ_M (μ_B). Indices i and s refer to interface and surface cations of the ML, respectively.

	Ti_2O_3	V_2O_3	Cr_2O_3	Fe_2O_3
d_s	0.80	0.69	0.63	0.61
d_i	0.88	0.93	1.01	0.90
Q_{Ms}	1.54	1.55	1.58	1.52
Q_{Mi}	2.02	1.85	1.73	1.73
Q_O	-1.28	-1.23	-1.22	-1.19
$Q_{Al_2O_3}$	0.27	0.30	0.35	0.30
μ_{Ms}	1.38	2.23	3.07	3.92
μ_{Mi}	0.49	1.69	2.79	-3.98

The mixing energies E_{mix} of the supported MM'O_3 monolayers are calculated from energy differences between the supported mixed oxide $E^{MM'O_3}$ and the average of the two corresponding supported parents $E^{M_2O_3}$ and $E^{M'_2O_3}$:

$$E^{MM'O_3}_{mix} = E^{MM'O_3} - \frac{E^{M_2O_3} + E^{M'_2O_3}}{2} \quad (1)$$

With this definition, mixing energies are negative if mixing is favoured.

3. Results on supported M_2O_3 monolayers

We first present the computational results for the M_2O_3 MLs supported on Al_2O_3. Table 1 and Figure 2 report their main structural, electronic, and magnetic characteristics. Corresponding results obtained with the HSE approach are given in SI, Tab. S2 and Fig. S2.

Since, in all cases, the supported ML structure is in the continuation of the corundum lattice with interface cations in the hollow site, the two cations of the oxide layers become strongly inequivalent. The interface ones have their full octahedral environment, while the surface cations are 3-fold coordinated. As a consequence, in the ML, the interlayer distance d_s between the surface cations and the oxygen plane is strongly reduced, in line with that found at all M-terminated M_2O_3(0001) surfaces (Tab S1 in SI, and references [46, 47, 48]). The interlayer distance d_i between the interface cations and the oxygen plane, on the other hand, is of the order of that found in bulk M_2O_3 along the (0001) direction (Tab S1 in SI).

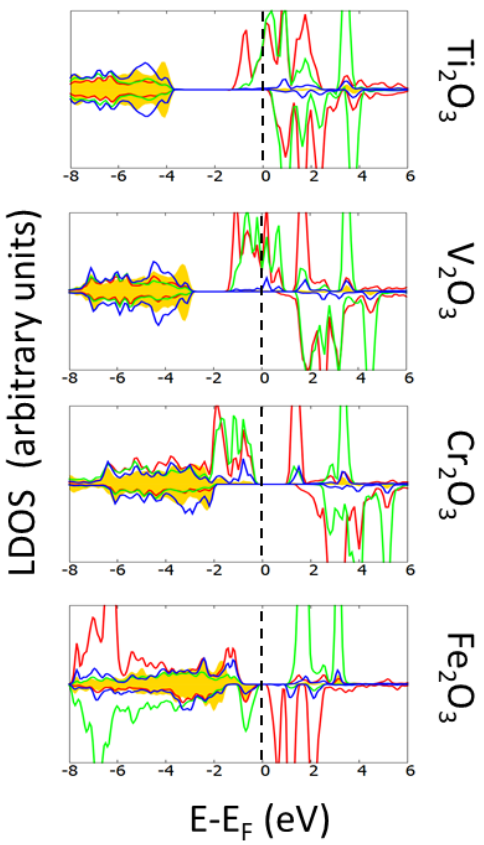

Figure 2. Local densities of states of Al_2O_3-supported M_2O_3 MLs projected on surface cations M_s (red), interface cations M_i (green), oxygen atoms O (blue), and substrate oxygen atoms (golden shading). Up and down spins are represented with positive and negative LDOS values, respectively. A broadening of 0.2 eV has been systematically applied. The vertical dashed lines indicate the positions of the Fermi levels. In the Al_2O_3-projected LDOS, the bottom of the CB, not visible at this scale, is located $\approx$ 4 eV above the VB maximum.

From an electronic point of view, in all cases, the substrate is positively charged, but the interfacial charge transfer is small, of the order of 0.3 e/M_2O_3 f.u. Indeed, as shown in Figure 2, stronger electron transfers cannot take place, because the M_2O_3 gap edges are sandwiched between those of Al_2O_3 (type I band offset). This is qualitatively different from the much larger electron transfers which take place at the interface between the same mixed oxide MLs and some metallic substrates [19]. In the present case, the interfacial charge transfer thus merely comes from the modifications of the iono-covalent character of interfacial bonds. In particular, the three subsurface O' atoms (Figure 1a) which have 3 Al and 1 TM neighbours have a charge which is reduced by $\approx$ 0.1 electron, with respect to that in Al_2O_3, due to the more covalent character of M-O bonds. This accounts nearly completely for the Al_2O_3 positive charging. Interestingly, in the only constituted interface involving Al_2O_3 that we have previously studied, namely Ti_2O_3/Al_2O_3 [15], the interfacial charge was nearly identical to that found in the present work, which confirms the very local character of this transfer.

In all cases, Fig. 2, the d states of the interface cations M_i occupy higher energy positions than those of the surface cations M_s, as a result of the larger Madelung potential generated by their octahedral environment. As a consequence, in contrast to their bulk counterparts, the Local Densities of States (LDOS) of Ti_2O_3 and V_2O_3 are metallic, due to an overlap of their interface and surface d states. Despite similar shifts, the LDOSs of Cr_2O_3 and Fe_2O_3 remain semiconducting but with a reduced gap width.

All magnetic structures are ferromagnetic, except Fe_2O_3 which is antiferromagnetic. The energy differences between the magnetic ground and excited states are 0.13 eV, 0.40 eV, 0.06 eV and 0.66 eV per unit cell in the series. The magnetic moments of interfacial and surface Cr and Fe cations are close to 3 and 4 μ_B, respectively, pointing to +3 oxidation states. The corresponding values for Ti and V depart from the respective values 1 and 2 μ_B expected for their +3 oxidation states, due to the metallic character of their band structures. This is not due to the interaction with the substrate, since the interfacial charge transfer is weak, but rather to an electron redistribution inside the ML layer, evidenced by the surface and interface LDOS overlap at the Fermi level E_F. This effect is much weaker in the HSE approach (SI Tab. S2 and Fig. S2).

4. Results on supported MM'O_3 monolayers

DFT+U results for the main structural, electronic and magnetic characteristics of Al_2O_3-supported mixed MM'O_3 MLs are given in Table 2. Figure 3 displays their LDOS in the two alternative cation configurations. Corresponding HSE results are given in SI, Table S3 and Figure S3.

Sitting in the prolongation of the Al_2O_3 lattice, all MM'O_3 MLs bear resemblance to an ilmenite M-O_3-M' (0001) trilayer (Fig. 1b). The two cations are not only chemically but also structurally distinct, due to their different coordination. Consequently, there are two inequivalent configurations with M at the interface and M' at the surface, or vice-versa. The preference for the location of a given cation is quantified by the energy difference $E_2 - E_1$ between the more stable configuration (Conf. #1) and the reverse one (Conf. #2) in Table 2. In the structural ground state Conf. #1, we find that the Fe cations systematically sit at the surface, while Cr cations preferentially occupy interface

Table 2. Main structural and electronic characteristics of Al_2O_3-supported mixed MM'O_3 monolayers in the more stable (Conf. #1) and less stable (Conf.#2) configurations: interplane distances d within the ML (Å), charges on cations Q_M, $Q_{M'}$ (e) and oxygen atoms Q_O (e), substrate charge $Q_{Al_2O_3}$ (e/surface unit cell), cation magnetic moments μ_M, $\mu_{M'}$ (μ_B), mixing energy E_{mix} and energy difference $E_2 - E_1$ between Conf. #2 and Conf. #1 (eV/surface unit cell). The cation formal charges, as deduced from the analysis of the electronic structure are indicated. M and M' refer to the first and second cation in the chemical formula, and indices i and s to interface and surface cations, respectively.

	$TiVO_3$	$TiCrO_3$	$TiFeO_3$	$VCrO_3$	$VFeO_3$	$CrFeO_3$
Conf. #1						
$d_M/d_{M'}$	0.82/0.88	0.70/1.02	0.84/0.69	0.67/1.00	0.87/0.69	0.97/0.61
$Q_M/\ Q_{M'}$	2.13/1.33	1.69/1.73	2.14/1.30	1.62/1.72	2.02/1.31	1.74/1.53
Q_O	-1.24	-1.27	-1.25	-1.23	-1.21	-1.21
$Q_{Al_2O_3}$	0.27	0.39	0.30	0.34	0.31	0.36
$\mu_M/\mu_{M'}$	0.13/2.75	1.03/2.79	0.08/3.59	2.05/2.82	1.04/3.61	2.63/-3.97
E_{mix}	-0.59	-0.56	-1.72	-0.04	-0.76	-0.43
Conf.	$Ti_i^{4+}V_s^{2+}$	$Ti_s^{3+}Cr_i^{3+}$	$Ti_i^{4+}Fe_s^{2+}$	$V_s^{3+}Cr_i^{3+}$	$V_i^{4+}Fe_s^{2+}$	$Cr_i^{3+}Fe_s^{3+}$
Conf. #2						
$d_M/d_{M'}$	0.76/0.96	0.84/0.82	0.73/0.95	0.91/0.72	0.64/0.95	0.62/0.93
$Q_M/Q_{M'}$	1.68/1.78	2.12/1.33	1.69/1.72	1.93/1.44	1.65/1.66	1.58/1.73
Q_O	-1.25	-1.24	-1.24	-1.23	-1.20	-1.19
$Q_{Al_2O_3}$	0.29	0.27	0.31	0.32	0.29	0.27
$\mu_M/\mu_{M'}$	0.97/1.88	0.18/3.76	0.92/4.05	1.43/3.52	1.82/3.93	2.80/-4.06
E_{mix}	-0.06	-0.32	-0.01	-0.01	+0.68	+0.51
Conf.	$Ti_s^{3+}V_i^{3+}$	$Ti_i^{4+}Cr_s^{2+}$	$Ti_s^{3+}Fe_i^{3+}$	$V_i^{3+}Cr_s^{3+}$	$V_s^{3+}Fe_i^{3+}$	$Cr_s^{3+}Fe_i^{3+}$
$E_2 - E_1$	0.53	0.24	1.71	0.03	1.44	0.94

sites, as do Ti cations in $TiVO_3$.

From an electronic point of view, and for the same reasons as for the M_2O_3 parents (type I interface), whatever the M and M' configuration, the charge transfer to the Al_2O_3 substrate is of the order of 0.3-0.4 e/surface unit cell, and due nearly entirely to the reduction of the subsurface O' charges.

In Conf. #1, all LDOSs are insulating except $VCrO_3$. The gap widths are small, nearly vanishing in some cases, but they open in the HSE approach (SI Fig. S3). Three mixed oxides display a clear cationic change of oxidation states compared to their parents, which may be considered as resulting from an actual redox process: $Ti^{4+}V^{2+}$, $Ti^{4+}Fe^{2+}$, and $V^{4+}Fe^{2+}$. These assignments are confirmed by the concomitant observation of 1) an increased charge of the first cation and a decreased charge of the second one; 2) the values of the magnetic moments: $\mu(Ti) \approx 0\mu_B$ characteristic of Ti^{4+}, $\mu(V) \approx 1\ \mu_B$ in $VFeO_3$ and $\approx 3\ \mu_B$ in $TiVO_3$ characteristic of V^{4+} and V^{2+}, respectively, and $\mu(Fe) \approx 3.6\ \mu_B$ characteristic of Fe^{2+}; and finally 3) the disappearance of the Ti peak below E_F, apparition of a Fe peak below E_F and correlative shifts of the V d state. In contrast, in $TiCrO_3$, $VCrO_3$ and $CrFeO_3$, there is no redox reaction and the cations keep their +3 oxidation state, with magnetic moments $\approx$ 1, 2, 3, and 4 μ_B for Ti, V, Cr and Fe, respectively.

Table 2 and Figure 3 (bottom panels) also display the structural and electronic characteristics of the less stable configurations (Conf. #2) in which the two TM cations of the MLs occupy reversed positions. The two most striking differences with respect to Conf. #1 are the absence of a redox process in $TiVO_3$, $TiFeO_3$ and $VFeO_3$ and its occurrence in $TiCrO_3$, as witnessed by the values of the magnetic moments and the shifts of the d states in the LDOSs (Fig. 3). The origin of these differences may be assigned to the different values of the Madelung potentials at surface and interface cationic sites, and will be further discussed in Section 5.1. The estimation of cation oxidation states is more difficult in $VCrO_3$, because of its quasi-metallic electronic structure with strong cation-cation orbital hybridization. As a result, the magnetic moments have intermediate values between 1 and 2 μ_B for V and between 3 and 4 μ_B for Cr. Nevertheless, thanks to the noticeable gap opening which takes place within the HSE approach, the magnetic moments approach 2 and 3 μ_B, respectively, which suggest a $V^{3+}Cr^{3+}$ configuration.

A favourable mixing is associated to negative values of the mixing energy E_{mix} (Equation 1). This is the case for all MM'O_3 MLs in their more stable state (Conf. #1) while positive or vanishingly small values are found for most MLs in Conf. #2. The only exception in the latter case is $TiCrO_3$ in which a redox process is observed. Let us note that, whatever the relative positions of the V and Cr cations, the mixing energy is close to zero in $VCrO_3$.

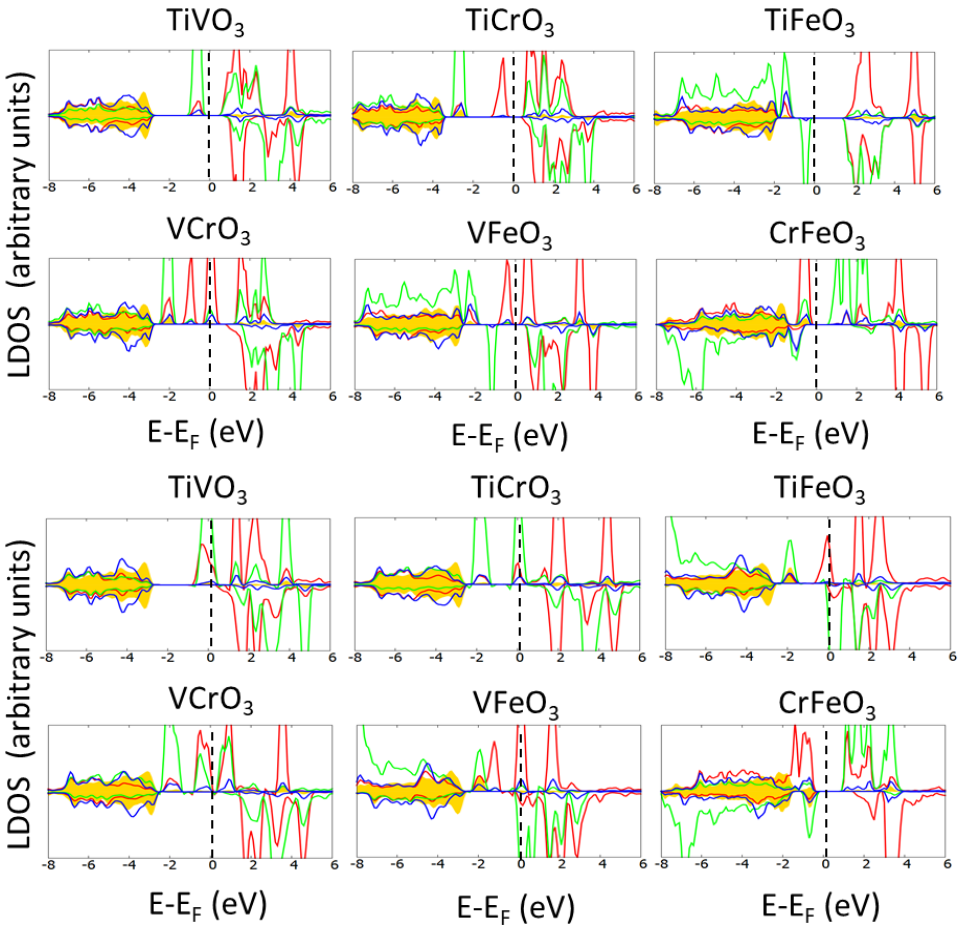

Figure 3. Local densities of states in Al_2O_3-supported mixed MM'O_3 MLs in Confs. #1 (top panels) and #2 (bottom panels), projected on M (red), M' (green), O atoms (blue), and substrate oxygen atoms (golden shading). A broadening of 0.2 eV has been systematically applied. Vertical dashed lines indicate the position of the Fermi level. In the Al_2O_3-projected LDOS, the bottom of the CB, not visible at this scale, is located $\approx$ 4 eV above the VB maximum.

5. Discussion

In this section, the existence or absence of cation-cation redox processes is rationalized by the consideration of the band offsets between the supported parents. Then, the two main contributions to the mixing energy are defined and discussed. Finally, in a broader perspective, the present findings are compared to the mixing characteristics of the same oxides in other morphologies or environments.

5.1. Mixing effect

According to the results of Section 4, an electron exchange between the two cations often occurs in mixed MLs, either small when due to orbital hybridization, or, in some cases, so strong that it results in a well-defined change of the cationic oxidation states. In our past studies of bulk [16] or free-standing ML [17] mixed oxides, we have shown that the latter effect may be qualitatively inferred from the relative positions of the parent band structures.

Figure 4 shows the cation projected LDOS of the four supported parent MLs, aligned with respect to the vacuum level (corresponding HSE result in SI Figure S4). The ordering of the Fermi levels $E_F(Ti_2O_3) > E_F(V_2O_3) > E_F(Fe_2O_3) > E_F(Cr_2O_3)$ suggests possible cation-cation electron transfers from the left to the right in this series (approximately from the least to the most electronegative cation), provided that the relevant DOSs in the energy window between the two Fermi levels are significant.

From this last viewpoint, redox effects are expected to be markedly different in the two possible cation configurations Conf #1 and Conf #2, since the d levels of surface and interface cations occupy different positions on the energy scale—higher position at interface due to stronger Madelung potential, lower position at surface due to a reduced coordination and thus a reduced Madelung potential. This is

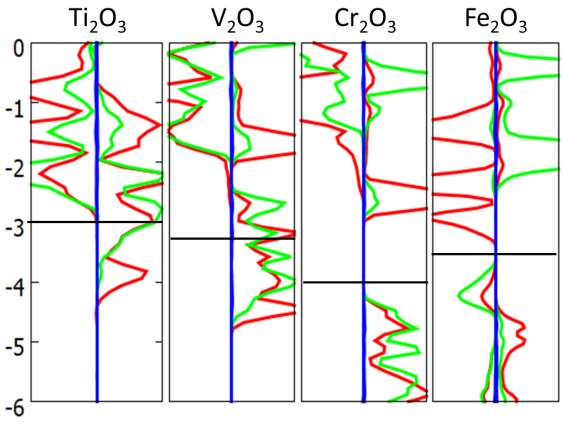

Figure 4. Local densities of states of Al_2O_3-supported M_2O_3 MLs projected on cations (red for surface, green for interface) and aligned with respect to the vacuum level. A broadening of 0.2 eV has been systematically applied. The horizontal lines indicate the positions of the Fermi levels.

convincingly exemplified in Cr- and Fe-containing mixed oxides, in which, according to Figure 4, a redox reaction upon mixing with Ti or V can only take place if the Cr and Fe cations are located at the surface. Indeed three among the four mixed oxides in which a redox process takes place, namely $Ti_iFe_sO_3$ (Conf. #1), $V_iFe_sO_3$ (Conf. #1) and $Ti_iCr_sO_3$ (Conf. #2) have this cation configuration and no redox is found when the cation positions are reversed. In $TiVO_3$ (Conf. #1), the band offset between the parent DOS also suggests a change of oxidation states, while in $VCrO_3$ (Conf. #1), and $CrFeO_3$ (Confs. #1 and #2) it correctly concludes to an absence of redox. It is quite remarkable that an argument which is still no more than a qualitative guideline allows predicting the occurrence or absence of a redox in ten among the twelve configurations under study.

5.2. Cation mixing and interface configurations

As a complement to the electronic properties discussed above, the value of the mixing energy E_{mix} quantifies the propensity of the two cations M and M' to mix in Al_2O_3-supported MM'O_3 MLs. The E_{mix} values may be analysed by splitting them into two main contributions:

$$E_{mix} = E_{mix}^{surf} + E_{mix}^{elec} \quad (2)$$

The first one E_{mix}^{surf} is associated to the structural non-equivalence of M and M' and, thus, to the cost of bond breaking when forming a surface. Considering the definition of E_{mix} (Equation 1), it may be approximated by the difference between the surface energies E_{surf} of M_2O_3(0001) and M'$_2O_3$(0001) slabs, i.e. $E_{mix}^{surf} = [E_{surf}(M_2O_3) - E_{surf}(M'_2O_3)]/2$ if M is at the surface and M' at the interface, or the negative of this quantity for cations in the alternative configuration. The second contribution E_{mix}^{elec} mainly involves electronic degrees of freedom and is expected to be large and negative when a redox reaction takes place. Table 3 displays the values of E_{mix} and its two contributions for the two cation configurations.

Table 3. Mixing energy E_{mix} in Al_2O_3-supported MM'O_3 MLs and its two contributions E_{mix}^{surf} and E_{mix}^{elec} (eV/surface unit cell), in Conf. #1 (left) and Conf. #2 (right) configurations. Bold fonts are used when a redox process takes place.

	E_{mix}	E_{mix}^{surf}	E_{mix}^{elec}	E_{mix}	E_{mix}^{surf}	E_{mix}^{elec}
$TiVO_3$	-0.59	0.07	**-0.66**	-0.06	-0.07	+0.01
$TiCrO_3$	-0.56	-0.21	-0.35	-0.32	+0.21	**-0.53**
$TiFeO_3$	-1.72	-0.10	**-1.62**	-0.01	+0.10	-0.11
$VCrO_3$	-0.04	-0.14	+0.10	-0.01	+0.14	-0.15
$VFeO_3$	-0.76	-0.17	**-0.59**	+0.68	+0.17	+0.51
$CrFeO_3$	-0.43	-0.32	-0.11	+0.51	+0.32	+0.19

As expected, most E_{mix}^{surf} contributions are negative in the most stable configuration Conf. #1, and positive otherwise. Since E_{surf} is equal to 2.19, 2.34, 2.62 and 2.00 eV/surface unit cell in the series from Ti to Fe (Table S1 in SI), E_{mix}^{surf} favours the location of Cr cations (the highest E_{surf}) at the interface and of Fe cations (the lowest E_{surf}) at the surface. This argument is in agreement with the positions of these cations in Conf. #1. Interestingly, a similar argument has been used in the literature when discussing doping effects in α-Al_2O_3 or TM oxides [49, 14]. The surface energy ordering $Fe_2O_3 < Ti_2O_3 < V_2O_3 < Al_2O_3 < Cr_2O_3$ is consistent with their conclusions that Fe dopants segregate at the surface of V_2O_3, Al_2O_3, and Cr_2O_3, while Cr dopants sit subsurface at Fe_2O_3, V_2O_3, and Al_2O_3 (0001) surfaces. According to the same mechanism, V dopants were shown to segregate at the surface of Cr_2O_3 and migrate subsurface on Fe_2O_3.

Regarding the electronic contribution to mixing, large negative values are found when a redox reaction unambiguously takes place, i.e. in $TiVO_3$, $TiFeO_3$ and $VFeO_3$ in Conf. #1, and in $TiCrO_3$ in Conf. #2. For eleven among the twelve mixed MLs, there is thus a definite strong correlation between the existence/absence of a cation-cation redox process and a large and negative/small or positive E_{mix}^{elec} value. It allows us to infer that, in the twelfth case (Conf. #2 of $VCrO_3$) for which the analysis of the DFT+U magnetic moments and LDOS did not allow to unambiguously conclude, indeed no redox takes place, considering the low value of E_{mix}^{elec}.

This discussion shows that the stability of mixed MLs with respect to their parents (negative value of E_{mix}) depends on the interplay between two very different driving forces, which may act concomitantly or in opposition to one another. Cation-cation redox reactions, in most cases, strongly stabilise mixed

configurations, but preference for a given cation position in the ML because of surface energy reasons may strengthen, weaken or even block the tendency to mixing. For example, in $TiCrO_3$ and $CrFeO_3$ (Conf. #1), in which the cations keep their +3 oxidation state, the mixing energies E_{mix} are relatively large and negative, but Table 3 shows that a large part of it is not of electronic origin but rather originates from E_{mix}^{surf}. In Conf. #2, the value of E_{mix} in $TiCrO_3$ may seem rather weak for a compound with a change of cation oxidation states, but Table 3 proves that it is due to an unfavourable surface energy effect, while the electronic contribution is of the same order as that in the Conf. #1 of $TiVO_3$ et $VFeO_3$.

5.3. Redox dependence on dimensionality and environment

The dependence of the mixing energy and redox properties on the cation positions evidenced in the preceding sections highlights their sensitivity to the local cation environment. To exemplify this effect more thoroughly, we now compare our present findings with results obtained previously for the same mixed oxides with different morphologies, namely the ilmenite bulk structure [16] or free-standing MLs [17]. What makes the comparison interesting is the progressive decrease of the mean cation coordination in the series from bulk (all cations are 6-fold coordinated), to Al_2O_3-supported MLs (interface and surface cations are 6- and 3- fold coordinated, respectively) and to free-standing MLs (all cations are 3-fold coordinated).

Table 4 provides a summary of the mixed oxides which display a strong mixing tendency associated to a cation redox process in these various systems. Beyond some differences between them which are related to the coordination dependence of the parent band offsets and the character of the band edges, a common bias for 6-fold coordinated Ti cations (Ti_i) to formally become Ti^{4+} is visible, which is associated with the high position of the filled Ti_i d state on the energy scale. Similarly, 3-fold coordinated Fe cations (Fe_s) easily transform into Fe^{2+} thanks to the low position of their empty d states. The table also highlights the existence of a change of oxidation state in $TiCrO_3$ (Conf. #2) which is specific to the Al_2O_3-supported ML.

We recall that a different mechanism is at work in MLs deposited on a metallic substrate [19]. There, we have shown that interfacial charge transfers are much larger than on Al_2O_3, so that the metal may play an active role in changes of cation oxidation states, whenever its Fermi level overlaps the oxide bands. On Ag(111), Au(111) and Pt(111), this occurs in supported Ti_2O_3 and V_2O_3 MLs and is even increased in some mixed MLs, such as $VCrO_3$ and $VFeO_3$.

Table 4. Mixed MM'O_3 oxides displaying a strong mixing tendency associated to a change of cation oxidation states, in various morphologies: bulk, Al_2O_3-supported ML (ML/Al_2O_3), free-standing ML (ML). The cation location is indicated by indices s and i which refer to surface and interface (or bulk), respectively.

	$TiVO_3$	$TiCrO_3$	$TiFeO_3$	$VFeO_3$
Bulk	Ti_iV_i	-	Ti_iFe_i	-
ML/Al_2O_3	Ti_iV_s	Ti_iCr_s	Ti_iFe_s	V_iFe_s
ML	-	-	Ti_sFe_s	V_sFe_s

These significant differences in the electronic structure of a given mixed oxide according to its dimensionality and/or the substrate it is in contact with, gives an additional lever to a doping strategy, in view of various applications. For example, in vanadium oxide catalysts, it is known that the oxidation state of the vanadium atoms plays a crucial role on its reactivity. The examples given in our present and past studies show that mixing with another TM sesquioxide may favour +3, +4, or +5 oxidation states, depending on the TM partner, the morphology and dimensionality of the mixed oxide and its environment.

6. Conclusion

Considering the growing importance of sub-monolayer TM oxides supported on another oxide in the chemical industry, we have used a DFT+U approach to study the properties of pure M_2O_3 and mixed MM'O_3 $3d$ transition metal oxide monolayers (M, M' = Ti, V, Cr, Fe) supported on an α-Al_2O_3(0001) support.

With their structure in the prolongation of the alumina corundum lattice, the MLs have non-equivalent surface and interface cations. Two different cation configurations thus exist in the mixed oxides. We have related the preference for one or the other to the relative values of the surface energies of the parent oxides.

In all cases, the interfacial charge transfer to the substrate is weak, but strong electron redistributions may take place between the cations in the mixed MLs, which lead to changes of cation oxidation states and can be described as actual redox processes. This is true in $TiVO_3$, $TiFeO_3$ and $VFeO_3$ in their most stable configurations, and in $TiCrO_3$ in the alternative configuration. We have deciphered the conditions under which redox processes occur, and shown that the band off-sets between the parent oxides are good guidelines to predict them.

The analysis of mixing energies has revealed that the stability of mixed MLs with respect to their parents depends on the interplay between two very different driving forces—tendency to a redox reaction and difference in surface energies—which may act

concomitantly or in opposition to one another.

Finally, by comparing the mixed oxide characteristics evidenced in the present study to those obtained previously in bulk ilmenite, in free-standing MLs, and in MLs deposited on transition metal substrates, we have highlighted the flexibility of their electronic structure as a function of size, dimensionality and nature of support. This suggests levers to tune TM oxide properties for specific applications.

7. Supporting Information Available

The Supporting Information contains:

(i) DFT+U results for bulk M_2O_3 corundum oxides and their (0001) surfaces (Tab. S1 and Fig. S1);

(ii) HSE results for Al_2O_3-supported M_2O_3 MLs and comparison with DFT+U results (Tab. S2 and Fig. S2);

(iii) HSE results for Al_2O_3-supported mixed MM'O_3 MLs in the two alternative cation configurations and comparison with DFT+U results (Tabs. S3 and Fig. S3);

(iv) HSE band alignment of Al_2O_3-supported M_2O_3 MLs and comparison with DFT+U results (Fig. S4).

This material is available free of charge via the Internet at ...

8. References

[1] Netzer F P and Noguera C 2021 *Oxide Thin Films and Nanostructures* (Oxford University Press)

[2] Bayati M, Molaei R, Narayan R, Narayan J, Zhou H and Pennycook S 2012 *Applied Physics Letters* **100** 251606

[3] Artiglia L, Agnoli S and Granozzi G 2015 *Coordination Chemistry Reviews* **301** 106–122

[4] Dillemans L, Smets T, Lieten R, Menghini M, Su C Y and Locquet J P 2014 *Applied Physics Letters* **104** 071902

[5] Pinho P V B, Chartier A, Moussy J B, Menut D and Miserque F 2020 *Materialia* **12** 100753

[6] Thevuthasan S, Kim Y, Yi S, Chambers S, Morais J, Denecke R, Fadley C, Liu P, Kendelewicz T and Brown Jr G 1999 *Surface Science* **425** 276–286

[7] Le H L T, Goniakowski J, Noguera C, Koltsov A and Mataigne J M 2016 *The Journal of Physical Chemistry C* **120** 9836–9844

[8] Le H L T, Goniakowski J, Noguera C, Koltsov A and Mataigne J M 2017 *The Journal of Physical Chemistry C* **121** 25143–25151

[9] Chamberlin S E, Kaspar T C, Bowden M E, Shutthanandan V, Kabius B, Heald S, Keavney D and Chambers S A 2014 *Journal of Applied Physics* **116** 233702

[10] Fallarino L, Binek C and Berger A 2015 *Physical Review B* **91** 214403

[11] Kramer A, Sutter E, Su D and Batzill M 2017 *Thin Solid Films* **631** 85–92

[12] Lantz G, Hajlaoui M, Papalazarou E, Jacques V L, Mazzotti A, Marsi M, Lupi S, Amati M, Gregoratti L, Si L *et al.* 2015 *Physical Review Letters* **115** 236802

[13] Jiang M, Mao J, Li X and Chen Z 2021 *International Journal of Hydrogen Energy* **46** 6693–6700

[14] Baltrusaitis J, Hatch C and Orlando R 2012 *The Journal of Physical Chemistry C* **116** 18847–18856

[15] Le H L, Goniakowski J and Noguera C 2019 *Surface Science* **679** 17–23

[16] Le H L T, Goniakowski J and Noguera C 2018 *Phys. Rev. Mat.* **2** 085001

[17] Goniakowski J and Noguera C 2019 *J. Phys. Chem. C* **123** 7898–7910

[18] Goniakowski J and Noguera C 2019 *J. Phys. Chem. C* **123** 9272–9281

[19] Goniakowski J and Noguera C 2020 *The Journal of Physical Chemistry C* **124** 8186–8197

[20] Surnev S, Sock M, Kresse G, Andersen J N, Ramsey M and Netzer F 2003 *The Journal of Physical Chemistry B* **107** 4777–4785

[21] Plessow P N, Bajdich M, Greene J, Vojvodic A and Abild-Pedersen F 2016 *The Journal of Physical Chemistry C* **120** 10351–10360

[22] Barcaro G, Agnoli S, Sedona F, Rizzi G A, Fortunelli A and Granozzi G 2009 *J. Phys. Chem. C* **113** 5721–5729 ISSN 1932-7447

[23] Pomp S, Kuhness D, Barcaro G, Sementa L, Mankad V, Fortunelli A, Sterrer M, Netzer F P and Surnev S 2016 *J. Phys. Chem. C* **120** 7629–7638

[24] Tumino F, Carrozzo P, Mascaretti L, Casari C S, Passoni M, Tosoni S, Bottani C E and Bassi A L 2015 *2D Materials* **2** 045011

[25] Wu C, Marshall M S J and Castell M R 2011 *J. Phys. Chem. C* **115** 8643–8652

[26] Wu C, Castell M R, Goniakowski J and Noguera C 2015 *Phys. Rev. B* **91** 155424

[27] Wang S, Hu X, Goniakowski J, Noguera C and Castell M R 2019 *Nanoscale* **11** 2412–2422

[28] Wang S, Goniakowski J, Noguera C and Castell M R 2019 *Physical Review B* **100** 125408

[29] Afonso J F and Pardo V 2015 *Phys. Rev. B* **92** 235102

[30] Köksal O, Baidya S and Pentcheva R 2018 *Phys. Rev. B* **97** 035126

[31] Kresse G and Furthmuller J 1996 *Phys. Rev. B* **54** 11169–11186

[32] Kresse G and Hafner J 1993 *Phys. Rev. B* **47** 558–561

[33] Blöchl P E 1994 *Phys. Rev. B* **50** 17953–17979

[34] Kresse G and Joubert D 1999 *Phys. Rev. B* **59** 1758–1775

[35] Dion M, Rydberg H, Schroder E, Langreth D C and Lundqvist B I 2004 *Phys. Rev. Lett.* **92** 246401

[36] Klimes J, Bowler D R and Michaelides A 2010 *J. Phys.: Cond. Matt.* **22** 022201

[37] Klimes J, Bowler D R and Michaelides A 2011 *Phys. Rev. B* **83** 195131

[38] Anisimov V I, Aryasetiawan F and Liechtenstein A I 1997 *J. Phys.: Condens. Matter* **9** 767–808

[39] Dudarev S L, Botton G A, Savrasov S Y, Humphreys C J and Sutton A P 1998 *Phys. Rev. B* **57** 1505–1509

[40] Heyd J, Scuseria G and Ernzerhof M 2003 *J. Chem. Phys* **118** 8207–8215

[41] Heyd J, Scuseria G and Ernzerhof M 2006 *J. Chem. Phys* **124** 219906–219906

[42] Bader R F W 1991 *Chem. Rev.* **91** 893–928

[43] Henkelman G, Arnaldsson A and Jonsson H 2006 *Comput. Mater. Sci.* **36** 354–360

[44] Momma K and Izumi F 2011 *J. Appl. Crystallogr.* **41** 1272–1276

[45] Monkhorst H and Pack J 1976 *Phys. Rev. B* **13** 5188–5192

[46] Paier J 2016 *Catalysis Letters* **146** 861–885

[47] Rohr F, Bäumer M, Freund H J, Mejias J, Staemmler V, Müller S, Hammer L and Heinz K 1997 *Surface Science* **372** L291–L297

[48] Kiejna A and Pabisiak T 2012 *Journal of Physics: Condensed Matter* **24** 095003

[49] Jonayat A, Kramer A, Bignardi L, Lacovig P, Lizzit S,

Van Duin A C, Batzill M and Janik M J 2018 *Physical Chemistry Chemical Physics* **20** 7073–7081